

DYNAMIC ANALYSIS OF FLEXIBLE MECHANICAL SYSTEMS USING LATDYN

by

Shih-Chin Wu
Che-Wei Chang
COMTEK
Grafton, VA 23662

and

Jerrold M. Housner
NASA Langley Research Center
Hampton, VA 23665

presented

at

3rd Annual Conference on Aerospace Computational Control
August 28-30, 1989 Oxnard, California

1. INTRODUCTION

Recently proposed space structures have grown increasingly large and complex. These may be delivered to orbit by the space shuttle and then deployed/assembled on orbit. To reduce weight, efficient designs of such systems tend to lead to flexible, low-frequency, and often joint-dominated structures. Interaction between rigid body motion and structural deformation will likely occur. For efficient operation of system requiring component articulation, it is desirable to maneuver components as rapidly as possible. Operational speed is limited by excessive dynamic deformation if vibrations are not suppressed. In order to suppress excessive vibration response, active controls may be utilized. The control design is usually based on linear methods, however the articulation is governed by nonlinear equations, moreover, design methods use reduced structural models. To access these design performance as well as stabilities, analytical simulations are usually performed.

Simulation codes for multibody systems such as DADS[1], DISCOS[2], and TREETOPS[3] use assumed mode approach to describe the structural deformations of components. This approach requires users to pick a reference frame for the component, discretize the component into finite elements, select component boundary conditions upon which the modes will be generated, solve the eigenvalue problem for deformation modes and select a modal set for the application at hand. Modal selection is often the most crucial part in the procedure. Since deformations of the component are defined as linear combination of the selected modes, the component can only deform in the space spanned by the selected modes. Therefore, results of the modal approach will be misleading if any modes are significantly excited were not selected. To predict which modes will get excited can be a difficult challenge in a flexible multibody system, since the system configurations are changing with time. Especially is thus true for many proposed future spacecrafts which have complicated geometry and joint hinges.

To provide an alternative approach which circumvented some of these difficulties, the LATDYN computer code was developed for research purposes. The LATDYN program is finite-element-based. The user model the component with finite elements, instead of using truncated modes which have to be generated outside the multibody analysis codes. In order to separate the rigid body motion and small deformations in the finite element approach, a coordinate system is chosen to represent the large displacement and rotation of the element. Deformations of the element are then defined with respect to the rigid body configuration of the element. At the element-level, mass matrices are calculated. The component mass matrix is obtained by assembling each elemental mass matrices as is typically done in conventional small motion/deformation finite element methods.

To form the system mass matrix, most multibody simulation codes impose nonlinear kinematic constraints on components that connect to the same joint. Instead of using constraint equations, the LATDYN program builds the hinge degree-of-freedom into the system equations of motion to connect components that share a common joint in a manner patterned after connectivity relations in conventional, small motion, finite elements. The mass of the interconnecting joint between the bodies represents a significant portion of the total mass and the orientation

of the joint's hinge lines play an important role in determining structural behavior. It is thus reasonable to construct the finite element program with the joints as a part of element connectivity.

2. KINEMATICS OF BEAM ELEMENT

The kinematics developed here is applicable to arbitrarily large displacement and rotational motion of a beam with small deformations. Consider the beam element with finite element nodes 1 and 2 at initial (undeformed) and current (deformed) configurations in an inertial X-Y-Z frame, as shown in Fig. 1. In order to specify the configuration of the beam element, it is necessary to define a set of generalized coordinates that uniquely define the global displacement of every point in the deformed element. For each node of the element, an $x_i-y_i-z_i$ ($i=1,2$) nodal reference frame having its x axis tangent to the neutral axis of the beam and y, z axes coincide with the principle axes of the beam cross section, is chosen to locate and orient the node in the inertia frame. Vectors r_i ($i=1,2$) from the origin of the initial $x_i-y_i-z_i$ nodal reference frame to the origin of the current $x_i-y_i-z_i$ nodal reference frame define the global displacement of nodes 1 and 2. Transformation matrices T_i from nodal reference frames to the global frame define orientations of the nodal reference frame. Deformation of the beam and displacement of any point in the beam now can be determined using r_i and T_i .

Before deformations of the beam can be defined, rigid body motion of the beam has to be separated from the large displacement of the beam. It is chosen to specify rigid body motion of the element by use of a convected coordinate system $X_C-Y_C-Z_C$ whose origin is located at node 1. Initially, orientations of the convected coordinate system coincides with the nodal reference frame of both nodes 1 and 2. As the element moves with large displacement and small deformation, the orientation of the convected coordinate frame, hence the rigid body motion of the beam, is determined by defining the X_C axis of the $X_C-Y_C-Z_C$ frame always lie along the line connecting nodes 1 and 2, and the Y_C axis to lie in the plane formed by the y axis of $x_1-y_1-z_1$ frame and the X_C axis of $X_C-Y_C-Z_C$ frame. With these definitions, the convected coordinate system is uniquely determined.

Deformations of the beam element are defined with respect to its rigid body configuration as

$$D_i = T_C^T T_i \quad (1)$$

where T_C denotes the transformation matrix from the rigid body configuration (or the convected coordinate frame) to the global frame. Where D_i is the difference in orientations between T_C and T_i at any time step, due to flexural deformation, namely, a transformation from T_C to T_i . Note that, D_i can also be regarded as the transformation of T_i that rotates about a vector from the undeformed states to the current states. Assume that the rotation angles between T_i and T_C are small, then the components of this vector are the three rotation angles measured with respect to the three axes of T_C [4]. Therefore, D_i can be simply represented by

$$D_i = \begin{bmatrix} 1 & -\phi_{zi} & \phi_{yi} \\ \phi_{zi} & 1 & -\phi_{xi} \\ -\phi_{yi} & \phi_{xi} & 1 \end{bmatrix}$$

where ϕ_{xi} , ϕ_{yi} , and ϕ_{zi} , are rotation angles of T_i about x, y, and z axis of T_c , respectively. Physically, they correspond to flexural deformations of the beam element at nodes 1 and 2.

The rotation angles may be readily extracted from D_i as follows:

$$\phi_{xi} = (0, 0, 1)D_i(0, 1, 0)^T \quad (2)$$

$$\phi_{yi} = (1, 0, 0)D_i(0, 0, 1)^T \quad (3)$$

$$\phi_{zi} = (0, 1, 0)D_i(1, 0, 0)^T \quad (4)$$

Substitution of Eq. 1 into Eqs.2-4 yields

$$\phi_{xi} = t_{c3}^T t_{i2} \quad (5)$$

$$\phi_{yi} = t_{c1}^T t_{i3} \quad (6)$$

$$\phi_{zi} = t_{c2}^T t_{i1} \quad (7)$$

where t_{cj} and t_{ij} are j th column of T_c and T_i , respectively. Since the x axis of T_c lies on the line connecting nodes 1 and 2, the direction cosines of the vector from nodes 1 to node 2, which is the first column of T_c , can be written as

$$t_{c1} = (x_2 - x_1 + x_0)/L \quad (8)$$

where x_0 is a vector from node 1 to node 2 in the initial configuration. Since the Y_c axis of T_c lies on the same plane formed by t_{c1} and t_{i2} , the Z_c axis of T_c , hence the third column of T_c , is the cross product of t_{c1} and t_{i2} , namely,

$$t_{c3} = \tilde{a} t_{c1} t_{i2} \quad (9)$$

The Y_c axis can be easily obtained by taking the cross product of t_{c3} and t_{c1} ,

$$t_{c2} = \tilde{a} t_{c3} t_{c1} \quad (10)$$

where \tilde{a} is the skew-symmetric matrix

$$\tilde{a} = \begin{bmatrix} 0 & -a_z & a_y \\ a_z & 0 & -a_x \\ -a_y & a_x & 0 \end{bmatrix}$$

with a_x, a_y, a_z being the vector components of vector \mathbf{a} . Note that $\tilde{\mathbf{a}}^T = -\tilde{\mathbf{a}}$ and that $\tilde{\mathbf{a}}\mathbf{b} = -\tilde{\mathbf{b}}\mathbf{a}$, which agrees with the vector product property $\mathbf{a} \times \mathbf{b} = -\mathbf{b} \times \mathbf{a}$.

Let $\rho = [x_C, y_C, z_C]$ be the position vector of an arbitrary point P in the beam element, defined with respect to T_C . Define that

$$\xi = x_C/L$$

$$\eta = y_C/L$$

$$\zeta = z_C/L$$

where L is the length of the beam element. The displacement of a point P on a beam element due to flexural deformation may be expressed as

$$\mathbf{u} = \mathbf{N}\Phi \quad (11)$$

where \mathbf{N} is a 3×6 matrix of shape functions similar to that used in the standard finite element method, namely

$$\mathbf{N} = \begin{bmatrix} 0 & (1-4\xi+3\xi^2)L\zeta & (-1+4\xi-3\xi^2)L\eta & 0 & (-2\xi+3\xi^2)L\zeta & (2\xi-3\xi^2)L\eta \\ -(1-\xi)L\zeta & 0 & (\xi-2\xi^2+\xi^3)L & -L\xi\zeta & 0 & (-\xi^2+\xi^3)L \\ -(1-\xi)L\eta & (-\xi+2\xi^2-\xi^3)L & 0 & -L\xi\eta & (\xi^2-\xi^3)L & 0 \end{bmatrix}$$

with ξ, η , and ζ being $x_C/L, y_C/L$, and z_C/L respectively, and Φ , the composite vector of rotation angles of nodes 1 and 2,

$$\Phi = [\phi_{x1}, \phi_{y1}, \phi_{z1}, \phi_{x2}, \phi_{y2}, \phi_{z2}]^T$$

The total displacement of point P as shown in Fig. 1 is, in vector form,

$$\vec{r}^P = \vec{r}_1 + \vec{\rho} + \vec{u} - \vec{\rho}_0$$

where ρ is the vector $[x_C, y_C, z_C]^T$ and in algebraic form,

$$\mathbf{r}^P = \mathbf{r}_1 + T_C \rho + T_C \mathbf{u} - T_{C0} \rho_0 \quad (12)$$

where T_{C0} is the initial transformation matrix of T_C and ρ_0 is the initial position vector of point P in T_C . Note that, axial deformation is implicitly included in the second term of the right-hand-side of Eq. 12.

3. SUPER-BEAM ELEMENT

In some multibody formulation, the joint connection between elements is imposed through constraint equations. Here, instead of introducing additional constraints, extra degree-of-freedom are added to the original element generalized coordinates to form a super beam-element consisting of joint and beam.

Consider a beam element with rigid joint bodies at both ends, as shown in Fig. 2. For simplicity, assume that no other element is attached to both joint bodies, and both joints have a one degree-of-freedom hinge. For each joint body, an $X_i-Y_i-Z_i$ ($i=1,2$) body reference frame is chosen to locate and orient the joint body in the inertia frame. Vectors R_i ($i=1,2$) from the origin of the initial body reference frame to the origin of the current body reference frame define the global displacement of joint bodies 1 and 2. Transformation matrices Γ_i from joint body reference frames to the global frame define orientations of the joint body. Vectors that locate joint attachment points in joint bodies are denoted s_i ($i=1,2$), defined with respect to joint body reference frames. Therefore, nodal displacements r_i of the beam element can be represented by the joint body displacements R_i as

$$r_i = R_i + \Gamma_i s_i - \Gamma_{i0} s_i \quad (13)$$

To determine the relation between T_i and Γ_i , consider coordinate systems $X_i'-Y_i'-Z_i'$ and $x_i'-y_i'-z_i'$ that are located at a joint attachment point one fixed to the joint body and one fixed to the nodal frame. Initially, let $X_i'-Y_i'-Z_i'$ and $x_i'-y_i'-z_i'$ coincide with the z axes parallel to the hinge axis. Then, the difference in orientations of both systems at any time is the relative rotation about the axis of hinge. The transformation matrix from $x_i'-y_i'-z_i'$ frame to $X_i'-Y_i'-Z_i'$ frame is

$$\Theta_i = \begin{bmatrix} \cos \theta_i & -\sin \theta_i & 0 \\ \sin \theta_i & \cos \theta_i & 0 \\ 0 & 0 & 1 \end{bmatrix}$$

where θ_i is the relative rotation angle. Denote Γ_i' and T_i' be the transformation matrices of $X_i'-Y_i'-Z_i'$ and $x_i'-y_i'-z_i'$ frames with respect to $X_i-Y_i-Z_i$ and $x_i-y_i-z_i$ frames, respectively. Then, the transformation matrix from joint body frame to the nodal reference frame can be obtained by sequential transformations as

$$T_i = \Gamma_i \Gamma_i' \Theta_i T_i' \quad (14)$$

Substituting Eqs. 13 and 14 into Eq. 12, the displacement of an arbitrary point in the beam can be represented in terms of displacements and orientations of joint bodies at the ends of beam element, and relative rotations of joint degrees-of-freedom, i.e.,

$$r^P = G(R_1, \Gamma_1, \theta_1, R_2, \Gamma_2, \theta_2) \quad (15)$$

4. VARIATIONAL EQUATIONS OF MOTION OF A SUPER-BEAM ELEMENT

The variational equations of motion of a beam element at time t , for a virtual displacement field that is consistent with the constraints is written as,

$$-\int_{\Omega} \mu \delta \mathbf{r}^P \ddot{\mathbf{r}}^P d\Omega + \int_{\Omega} \delta \mathbf{r}^P \mathbf{f}^P d\Omega + \int_{\sigma} \delta \mathbf{r}^P \mathbf{h}^P d\sigma = \int_{\Omega} \delta \epsilon^P \boldsymbol{\tau}^P d\Omega \quad (16)$$

where $\delta \mathbf{r}^P$ is a virtual displacement of point P that is consistent with constraints, $\ddot{\mathbf{r}}^P$ is the acceleration of point P, \mathbf{f}^P is body force density at point P, \mathbf{h}^P is the surface traction at point P, $\delta \epsilon^P$ is a kinematically compatible strain variation vector, $\boldsymbol{\tau}^P$ is the associated stress vector at point P, and Ω and σ are the volume and surface of the beam before it is deformed.

By taking the variation of Eq. 15, the virtual displacement of point P is obtained as

$$\delta \mathbf{r}^P = \mathbf{g}_{R_1} \delta R_1 + \mathbf{g}_{\Gamma_1} \delta \pi_1 + \mathbf{g}_{\theta_1} \delta \theta_1 + \mathbf{g}_{R_2} \delta R_2 + \mathbf{g}_{\Gamma_2} \delta \pi_2 + \mathbf{g}_{\theta_2} \delta \theta_2 \quad (17)$$

where $\delta \pi_i$ is virtual rotation of Γ_i . Therefore, the virtual displacement of a point P in the beam element is represented by the virtual displacements and rotations of the joint bodies, and virtual rotations of relative joint degrees-of-freedom.

The acceleration vector of a typical point can be obtained by taking two time derivatives of Eq. 15, which gives

$$\begin{aligned} \ddot{\mathbf{r}}^P = & \mathbf{g}_{R_1} \ddot{R}_1 + \mathbf{g}_{\Gamma_1} \dot{\omega}_1 + \mathbf{g}_{\theta_1} \ddot{\theta}_1 + \mathbf{g}_{R_2} \ddot{R}_2 + \mathbf{g}_{\Gamma_2} \dot{\omega}_2 + \mathbf{g}_{\theta_2} \ddot{\theta}_2 \\ & + \dot{\mathbf{g}}_{R_1} \dot{R}_1 + \dot{\mathbf{g}}_{\Gamma_1} \omega_1 + \dot{\mathbf{g}}_{\theta_1} \dot{\theta}_1 + \dot{\mathbf{g}}_{R_2} \dot{R}_2 + \dot{\mathbf{g}}_{\Gamma_2} \omega_2 + \dot{\mathbf{g}}_{\theta_2} \dot{\theta}_2 \end{aligned} \quad (18)$$

where ω_i and $\dot{\omega}_i$ are angular velocity and angular acceleration of the joint body i.

Substituting Eqs. 17 and 18 into Eq. 16, the first term is

$$\begin{aligned} & -\int_{\Omega} \mu \delta \mathbf{r}^P \ddot{\mathbf{r}}^P d\Omega \\ & = -[\delta R_1^T, \delta \pi_1^T, \delta \theta_1, \delta R_2^T, \delta \pi_2^T, \delta \theta_2] \left\{ \mathbf{M} \begin{bmatrix} \ddot{R}_1 \\ \dot{\omega}_1 \\ \ddot{\theta}_1 \\ \ddot{R}_2 \\ \dot{\omega}_2 \\ \ddot{\theta}_2 \end{bmatrix} + \mathbf{S}(\dot{R}_1, \omega_1, \dot{\theta}_1, \dot{R}_2, \omega_2, \dot{\theta}_2) \right\} \end{aligned} \quad (19)$$

where \mathbf{M} is the generalized mass matrix,

$$\mathbf{M} = \int_{\Omega} \mu \begin{bmatrix} \mathbf{g}_{R_1}^T \mathbf{g}_{R_1} & \mathbf{g}_{R_1}^T \mathbf{g}_{\Gamma_1} & \mathbf{g}_{R_1}^T \mathbf{g}_{\theta_1} & \mathbf{g}_{R_1}^T \mathbf{g}_{R_2} & \mathbf{g}_{R_1}^T \mathbf{g}_{\Gamma_2} & \mathbf{g}_{R_1}^T \mathbf{g}_{\theta_2} \\ & \mathbf{g}_{\Gamma_1}^T \mathbf{g}_{\Gamma_1} & \mathbf{g}_{\Gamma_1}^T \mathbf{g}_{\theta_1} & \mathbf{g}_{\Gamma_1}^T \mathbf{g}_{R_2} & \mathbf{g}_{\Gamma_1}^T \mathbf{g}_{\Gamma_2} & \mathbf{g}_{\Gamma_1}^T \mathbf{g}_{\theta_2} \\ & & \mathbf{g}_{\theta_1}^T \mathbf{g}_{\theta_1} & \mathbf{g}_{\theta_1}^T \mathbf{g}_{R_2} & \mathbf{g}_{\theta_1}^T \mathbf{g}_{\Gamma_2} & \mathbf{g}_{\theta_1}^T \mathbf{g}_{\theta_2} \\ & & & \mathbf{g}_{R_2}^T \mathbf{g}_{R_2} & \mathbf{g}_{R_2}^T \mathbf{g}_{\Gamma_2} & \mathbf{g}_{R_2}^T \mathbf{g}_{\theta_2} \\ & & & & \mathbf{g}_{\Gamma_2}^T \mathbf{g}_{\Gamma_2} & \mathbf{g}_{\Gamma_2}^T \mathbf{g}_{\theta_2} \\ & \text{Symmetric} & & & & \mathbf{g}_{\theta_2}^T \mathbf{g}_{\theta_2} \end{bmatrix} d\Omega$$

and \mathbf{S} is quadratic in velocity,

$$\mathbf{S} = \int_{\Omega} \mu \begin{bmatrix} \mathbf{g}_{R_1}^T (\dot{\mathbf{g}}_{R_1} \dot{\mathbf{R}}_1 + \dot{\mathbf{g}}_{\Gamma_1} \dot{\omega}_1 + \dot{\mathbf{g}}_{\theta_1} \dot{\theta}_1 + \dot{\mathbf{g}}_{R_2} \dot{\mathbf{R}}_2 + \dot{\mathbf{g}}_{\Gamma_2} \dot{\omega}_2 + \dot{\mathbf{g}}_{\theta_2} \dot{\theta}_2) \\ \mathbf{g}_{\Gamma_1}^T (\dot{\mathbf{g}}_{R_1} \dot{\mathbf{R}}_1 + \dot{\mathbf{g}}_{\Gamma_1} \dot{\omega}_1 + \dot{\mathbf{g}}_{\theta_1} \dot{\theta}_1 + \dot{\mathbf{g}}_{R_2} \dot{\mathbf{R}}_2 + \dot{\mathbf{g}}_{\Gamma_2} \dot{\omega}_2 + \dot{\mathbf{g}}_{\theta_2} \dot{\theta}_2) \\ \mathbf{g}_{\theta_1}^T (\dot{\mathbf{g}}_{R_1} \dot{\mathbf{R}}_1 + \dot{\mathbf{g}}_{\Gamma_1} \dot{\omega}_1 + \dot{\mathbf{g}}_{\theta_1} \dot{\theta}_1 + \dot{\mathbf{g}}_{R_2} \dot{\mathbf{R}}_2 + \dot{\mathbf{g}}_{\Gamma_2} \dot{\omega}_2 + \dot{\mathbf{g}}_{\theta_2} \dot{\theta}_2) \\ \mathbf{g}_{R_2}^T (\dot{\mathbf{g}}_{R_1} \dot{\mathbf{R}}_1 + \dot{\mathbf{g}}_{\Gamma_1} \dot{\omega}_1 + \dot{\mathbf{g}}_{\theta_1} \dot{\theta}_1 + \dot{\mathbf{g}}_{R_2} \dot{\mathbf{R}}_2 + \dot{\mathbf{g}}_{\Gamma_2} \dot{\omega}_2 + \dot{\mathbf{g}}_{\theta_2} \dot{\theta}_2) \\ \mathbf{g}_{\Gamma_2}^T (\dot{\mathbf{g}}_{R_1} \dot{\mathbf{R}}_1 + \dot{\mathbf{g}}_{\Gamma_1} \dot{\omega}_1 + \dot{\mathbf{g}}_{\theta_1} \dot{\theta}_1 + \dot{\mathbf{g}}_{R_2} \dot{\mathbf{R}}_2 + \dot{\mathbf{g}}_{\Gamma_2} \dot{\omega}_2 + \dot{\mathbf{g}}_{\theta_2} \dot{\theta}_2) \\ \mathbf{g}_{\theta_2}^T (\dot{\mathbf{g}}_{R_1} \dot{\mathbf{R}}_1 + \dot{\mathbf{g}}_{\Gamma_1} \dot{\omega}_1 + \dot{\mathbf{g}}_{\theta_1} \dot{\theta}_1 + \dot{\mathbf{g}}_{R_2} \dot{\mathbf{R}}_2 + \dot{\mathbf{g}}_{\Gamma_2} \dot{\omega}_2 + \dot{\mathbf{g}}_{\theta_2} \dot{\theta}_2) \end{bmatrix} d\Omega$$

Similarly, the second and third term in Eq. 16 become

$$\begin{aligned} & \int_{\Omega} \delta \mathbf{r}^P \mathbf{f}^P d\Omega + \int_{\sigma} \delta \mathbf{r}^P \mathbf{h}^P d\sigma \\ &= [\delta \mathbf{R}_1^T, \delta \pi_1^T, \delta \theta_1, \delta \mathbf{R}_2^T, \delta \pi_2^T, \delta \theta_2] \mathbf{Q} \end{aligned} \quad (20)$$

where \mathbf{Q} is the external generalized force vector,

$$\mathbf{Q} = \int_{\Omega} \begin{bmatrix} \mathbf{g}_{R_1}^T \mathbf{f}^P \\ \mathbf{g}_{\Gamma_1}^T \mathbf{f}^P \\ \mathbf{g}_{\theta_1}^T \mathbf{f}^P \\ \mathbf{g}_{R_2}^T \mathbf{f}^P \\ \mathbf{g}_{\Gamma_2}^T \mathbf{f}^P \\ \mathbf{g}_{\theta_2}^T \mathbf{f}^P \end{bmatrix} d\Omega + \int_{\sigma} \begin{bmatrix} \mathbf{g}_{R_1}^T \mathbf{h}^P \\ \mathbf{g}_{\Gamma_1}^T \mathbf{h}^P \\ \mathbf{g}_{\theta_1}^T \mathbf{h}^P \\ \mathbf{g}_{R_2}^T \mathbf{h}^P \\ \mathbf{g}_{\Gamma_2}^T \mathbf{h}^P \\ \mathbf{g}_{\theta_2}^T \mathbf{h}^P \end{bmatrix} d\sigma$$

For a Bernoulli beam, the right hand side of Eq. 16, or the virtual work done by the internal force, may be expressed as

$$\int_{\Omega} \delta \epsilon^P \tau^P d\Omega$$

$$\begin{aligned}
&= \int_0^L \{EAu_1 \delta u_1 + EI_y u_2'' \delta u_2'' + EI_z u_3'' \delta u_3'' + GJ \phi_{x_2} \delta \phi_{x_2}\} dx_c \\
&= [\delta R_1^T, \delta \pi_1^T, \delta \theta_1, \delta R_2^T, \delta \pi_2^T, \delta \theta_2] U
\end{aligned} \tag{21}$$

where u_1 is the axial deformation,

$$u_1 = \sqrt{(\mathbf{r}_2 - \mathbf{r}_1 + \mathbf{r}_0)^T (\mathbf{r}_2 - \mathbf{r}_1 + \mathbf{r}_0)} - \sqrt{\mathbf{r}_0^T \mathbf{r}_0}$$

u_2 and u_3 are bending displacements in the y and z direction of the neutral axis, which can be obtained from Eq. 11, and U is the generalized internal force vector.

Substituting Eqs. 19-21 into Eq. 16, the variational equation of motion of a super-beam element can be written as

$$[\delta R_1^T, \delta \pi_1^T, \delta \theta_1, \delta R_2^T, \delta \pi_2^T, \delta \theta_2] \mathbf{M} \begin{bmatrix} \ddot{\mathbf{R}}_1 \\ \dot{\omega}_1 \\ \ddot{\theta}_1 \\ \ddot{\mathbf{R}}_2 \\ \dot{\omega}_2 \\ \ddot{\theta}_2 \end{bmatrix} + \mathbf{S}(\dot{\mathbf{R}}_1, \omega_1, \dot{\theta}_1, \dot{\mathbf{R}}_2, \omega_2, \dot{\theta}_2) + \mathbf{U} - \mathbf{Q} = 0$$

for all virtual displacements δR_1 and δR_2 , virtual rotations $\delta \pi_1$ and $\delta \pi_2$, and virtual hinge rotations $\delta \theta_1$ and $\delta \theta_2$ that are consistent with the constraints.

5. APPLICATIONS

5.1.1 Analysis of A Deployable Space Structure

The deployable space structure shown in Fig. 3 is a 20 meter long, triangular cross section, joint dominated truss structure, referred to as the Mini-Mast. The structure is used at NASA Langley as a ground test article for the development of research techniques in structural dynamic characterization of large space structures and control of flexible structures. A total of 18 bays, each 1.12 meter long, make up the 20 meter length of the beam above the deployer mechanism. Figure 4 illustrates two deployed bays of the beam design in more detail. One bay of the truss beam consists of three longerons, three diagonal members and a batten triangular truss whose cross-section fits inside a 1.4 m diameter circle. The longerons and diagonal members are connected to batten triangles at each corner (three corner bodies are built into each corner of the batten triangle) by revolute joints. A sketch of a corner body is shown in Fig. 5, primarily to indicate geometric complexity.

The system is deployed/retracted with two bays at a time. During deploying/retraction, the vertices of two batten triangles are held

fixed in orientation while a third batten triangle, located between the two fixed ones, rotates about the longitudinal axis. Upward/downward forces are then applied to deploy/retract the system. Revolute joints in corner bodies at each apex of the triangular cross-section of each bay and a nearly over-center hinge in each diagonal member allow the beam truss to deploy/fold into a repeatable beam/stack, as shown in Fig. 4. At the final stage of deploying, mid-hinge of the diagonal member is locked up to ensure that the system becomes a structure. It is reopened as retraction starts. Since each two deploying bays are symmetric to the middle batten triangle, it is sufficient to analyze only one bay of the system.

The objective of the analysis is to determine loadings on flexible members during deployment of one bay of the truss beam. Because of the symmetric geometry of the system, corner bodies are constrained to move on a 1.4 m diameter cylinder during deployment. The longerons and diagonal members are deformed, due to kinematic constraints imposed at the joints, during deployment. Therefore, orientations of revolute joints of the longeron and diagonal member play an important role in design of the truss beam. A set of properly designed revolutes will decrease deformations, hence decreasing the force required to deploy the truss beam. The system is designed such that it is not deformed in its fully retracted position and this then serves as a good starting point to analyze the system response during deployment.

5.1.2 LATDYN Model Description

The model can be simplified by taking the advantage of symmetric geometry of triangular cross section of the system. By constraining the upper triangle to only move along and rotate about the longitudinal axis of the truss, the LATDYN model of one bay of Mini-Mast reduces to 3 flexible longerons, 3 flexible diagonal members, and 2 batten triangles that are modelled as rigid bodies, as shown in Fig. 6. The lower batten triangle, batten triangle A in Fig. 6, is grounded. The upper batten triangle, batten triangle B in Fig. 6, is driven up and down. The batten triangles are connected to the longerons and diagonal members with revolute joints at each corner, respectively. The geometry and material properties of the longeron and diagonal members are listed in Table 1. Initial configuration of the model is chosen with the system in its fully packaged position, as shown in Fig. 6. Locations and orientations of each revolute joints of longeron and diagonal member are listed in Tables 2 and 3, respectively.

5.1.3 Results

The system is deployed by driving the upper triangle in the longitudinal direction without constraining its rotation about the longitudinal axis. The driving constraint is

$$Z = \frac{L}{T} \left[t - \frac{T}{2\pi} \sin \left(\frac{2\pi t}{T} \right) \right], \quad t < T$$

$$Z = L, \quad t \geq T$$

where L is length of the longeron, T is total deploying time, and Z is the height of the upper triangle. The deployment moves the upper triangle a distance L in the z direction in T seconds. In the simulations which follow, T is taken as 1.0 second.

Figures 7-8 show the variations of the bending and twisting moments of the longeron at its midpoint, with the z displacement of the upper triangle. Figures 9-10 show the bending moments of diagonal member A and B while figures 11-13 display the time history of the axial forces of longeron and diagonal member, showing that all truss members in the system are actually in compression after deployed. This tends to increase bending stiffness of the truss beam. Figure 14 shows the LATDYN results for the bending moments of the longeron at the end joining the upper triangle. Also shown are the predictions of the Astro Co.[8]- the original Mini-Mast designer and producer, and the best result authors can achieve using the assumed mode approach. In Fig. 14, both LATDYN and Astro results predict a minimum bending moment in the longeron when it rotates about 50 degrees which is reasonable from the geometry of the structure. Results from the assumed mode approach indicate that the deformation modes used in the analysis are not complete, which is not apparent without another analysis test results.

5.2.1 Flapping Motion of Rotor Blade

A number of problems arise which make it necessary to study the effects of flexibility on blade motion. For example, the affect of flexible motion on the performance, stresses occur in the deformed blade, and interactions between the rotational speed and the natural frequencies of the flexible blade. An additional complicating factor is that due to the stiffening effect of centrifugal force, natural frequencies of the blade increase as blade rotation speed increases.

A simplified model of an articulated blade with no flap hinge offset or spring restraint is shown in Fig. 15. Initially, the blade is straight and tilted 0.157 radian. With no initial hinge velocity, the blade rotates at a constant speed. Since the centrifugal force always acts radially outward in a plane normal to the rotation axis, it acts as a spring force opposing the blade flap motion, hence initiating the flap motion and deformation.

Simulation of the same flapping blade, using an assumed mode approach, producing a diverging solution as is reported in Reference 5. This is because the geometric stiffening effect is not properly accounted for[6][7].

5.2.2 LATDYN Model and Results

In the simulation of the flapping blade using LATDYN, Rotation speed of the blade is kept constant in each simulation and gradually increased in succeeding simulations, starting with 1 rad/sec and going up to 9 rad/sec. Frequencies are calculated from the transient response of the simulation using a Fast Fourier Transform.

Figures 16 and 17 show the bending moment of the blade at the midpoint when it rotates at 3 and 6 rad/sec. The results clearly indicate that the natural frequency of the first flapping bending mode increases as the rotation speed increases, due to the centrifugal stiffening effect. Figure 18 displays natural frequencies of the first bending modes for different rotation speeds, compared to the solutions derived by Southwell [9]. Good agreement between the LATDYN results and the Southwell solution is shown: Also shown (dotted lines) in Fig. 18 are different harmonics of the rotor speed. As shown, the natural

frequency of the first mode intersects with the third harmonic around 8 rad/sec, fourth harmonic around 4 rad/sec, fifth harmonic around 3 rad/sec, and so on for higher harmonics. A resonance may then occur when the blade rotates around these speeds. Figure 19 shows the bending moment of the blade when it rotates at 8 rad/sec, which show that the magnitude of the bending blade keeps increasing with time. The frequency of the blade is about three times the rotational speed. The magnitude of the response in Fig. 19 may not increase indefinitely, but may represent a beating phenomenon with the period of the beat depending on the closeness of 8 rad/sec to the intersection point.

CONCLUSIONS

A three dimensional, finite element based simulation tool for flexible multibody systems is presented. Hinge degrees-of-freedom is built into equations of motion to reduce geometric constraints. The approach avoids the difficulty in selecting deformation modes for flexible components by using assumed mode method. The tool is applied to simulate a practical space structure deployment problem. Results of examples demonstrate the capability of the code and approach.

REFERENCES

1. Yoo, W. S., and Haug, E. J., "Dynamics of Articulated Structures, Part I: Theory and Part II: Computer Implementation and Applications", Journal of Structure Mechanics, Vol. 14, 1986, pp.105-126 and pp.177-189.
2. Bodley, C. S., Devers, A. D., Park, A. C., and Frisch, H. P., "A Digital Computer Program for the Dynamic Interaction Simulation of Controls and Structure (DISCOS)", Vols. 1 & 2, NASA Technical Paper 1219, May 1978.
3. Singh, R. P., VanderVoort, R. J., and Likins, P. W., "Dynamics of Flexible Bodies in Tree Topology - A Computer Oriented Approach", Paper No. AIAA-84-1024, AIAA/ASME/ASCE 25th Structural Dynamics and Materials Conf., Palm Springs, Ca, May 14-18, 1984.
4. Goldstein, H., Classical Mechanics, 2nd edition, Addison-Wesley Publishing Co., 1980.
5. Wu, S. C., A Substructure Method for Dynamic Simulation of Flexible Mechanical Systems with Geometric Nonlinearities, Ph.D Dissertation, University of Iowa, Iowa City, IA, 1987.
6. Kane, T. R., Ryan, R. R., and Banerjee, A. K., "Dynamics of A Beam Attached to a Moving Base", AAS/AIAA Astrodynamics Specialist Conference, Vail, Colorado, Aug. 12-15, 1985.
7. McGowan, P. E. and Housner, J. M., "Nonlinear Dynamic Analysis of Deploying Flexible Space Booms", NASA TM-87617, September, 1985.
8. Adams, L. R., "Design, Development and Fabrication of A Deployable/Retractable Truss Beam Model for Large Space Structures Application", NASA CR-178287, June 1987.
9. Bramwell, A. R. S., Helicopter Dynamics, John Wiley & sons, New York, 1976.

Table 1 Geometry and Material Properties

	Inner Diameter	Outer Diameter
Longeron	0.01491 m	0.02019 m
Diag. Member	0.01115 m	0.01511 m
Modulus of Elasticity = $1.17E+11$ N/m ²		
Shear Modulus of Elasticity = $4.0E+9$ N/m ²		
Density = $1.616E+3$ kg/m ³		

Table 2 Joints Location

Joint Name	X	Y	Z
Longeron A1	-0.60598	-0.34987	0.02379
Longeron B1	-0.23372	0.65954	0.02379
Diagonal A1	-0.58031	-0.34987	0.02379
Diagonal B2	-0.49966	-0.50693	0.02379
Diagonal A1B2	-0.14861	0.26657	0.02379

Table 3 Joints Orientations

Joint Name	X-component	Y-component	Z-component
Longeron A1	0.91838	0.07838	0.38786
Longeron B1	0.64757	-0.65591	-0.38786
Diagonal A1	0.98896	0.09973	-0.10956
Diagonal B2	0.88133	-0.39542	-0.25868
Diagonal A1B2	-0.88076	0.47339	0.01163

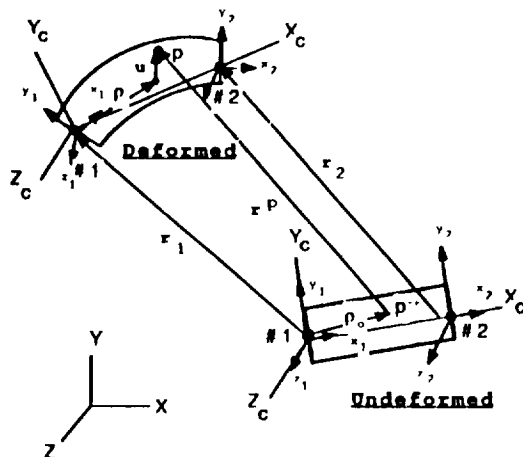


Figure 1 Kinematics of Beam Element

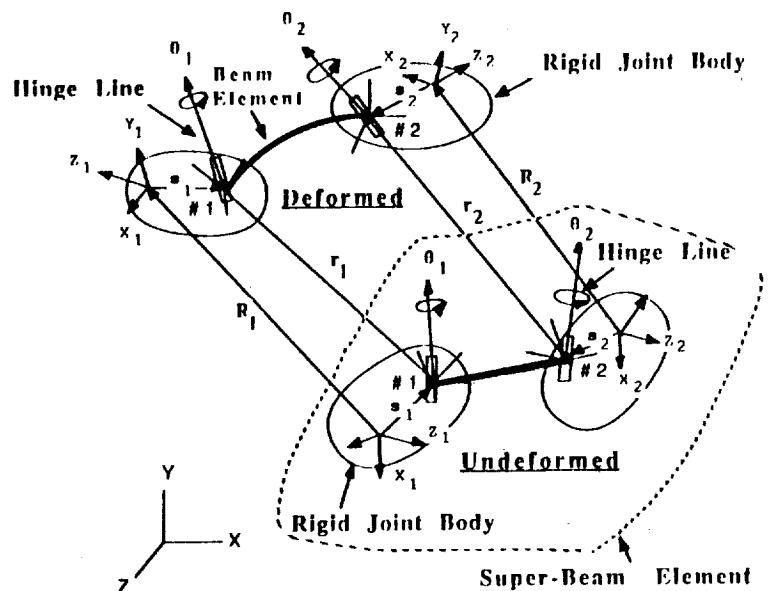


Figure 2 Kinematics of Super-Beam Element

ORIGINAL PAGE IS
OF POOR QUALITY

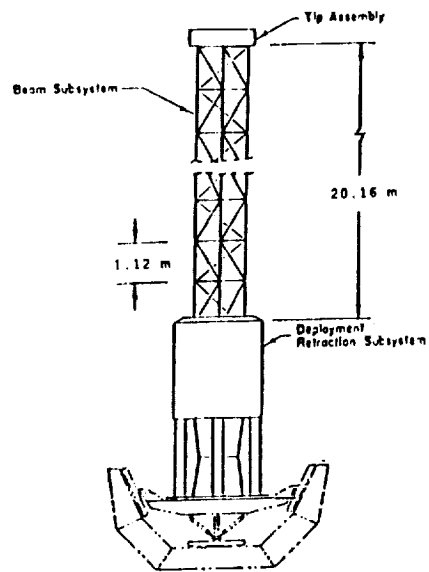


Figure 3 A Deployable Space Structure

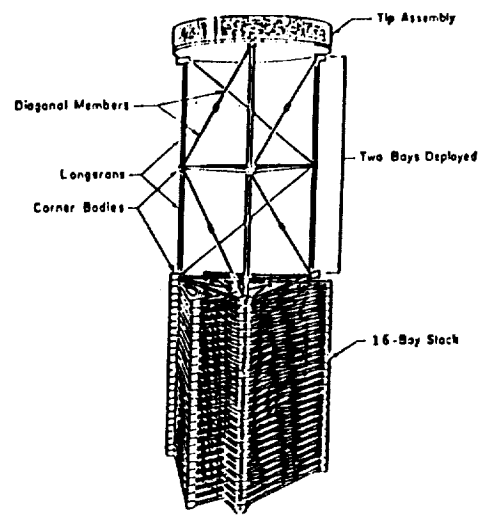


Figure 4 Two Bays Deployed

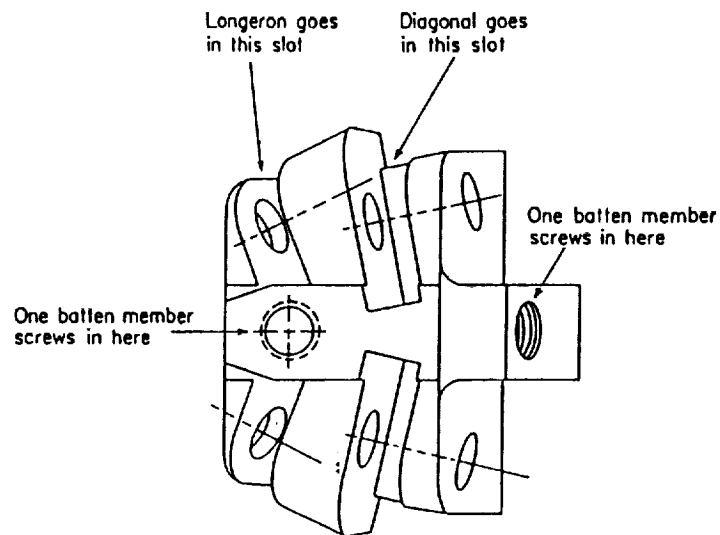
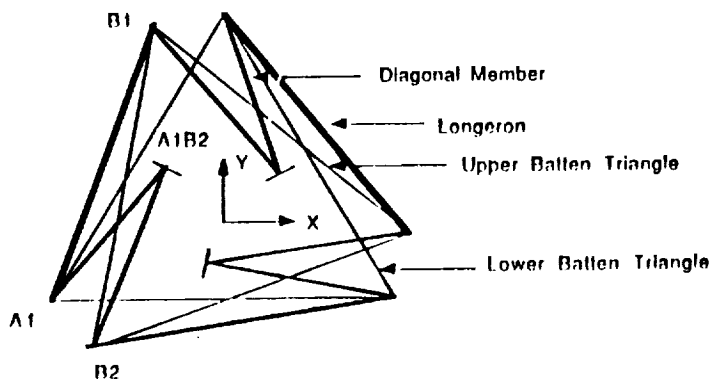
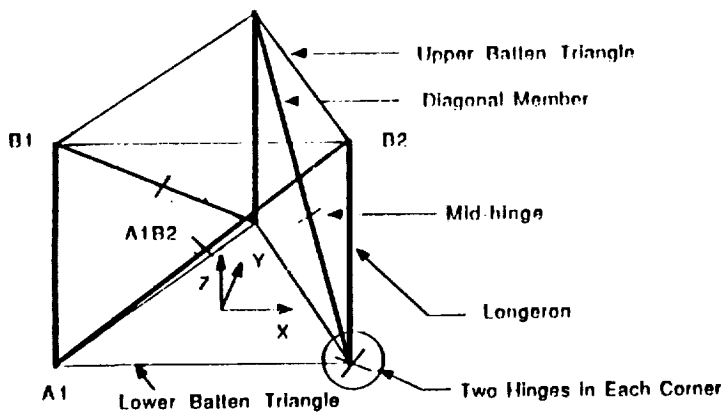


Figure 5 A Corner Body

ORIGINAL PAGE IS
OF POOR QUALITY



PACKAGED (Top View)



DEPLOYED

Figure 6 One Bay of Minimast

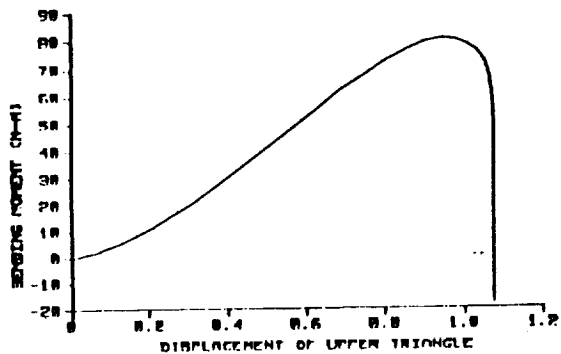


Figure 9 Bending Moment of Diagonal A at Midpoint

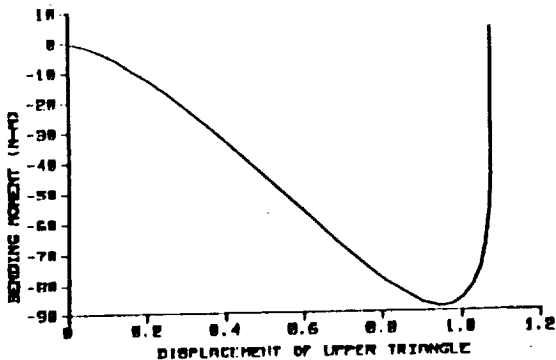


Figure 10 Bending Moment of Diagonal B at Midpoint

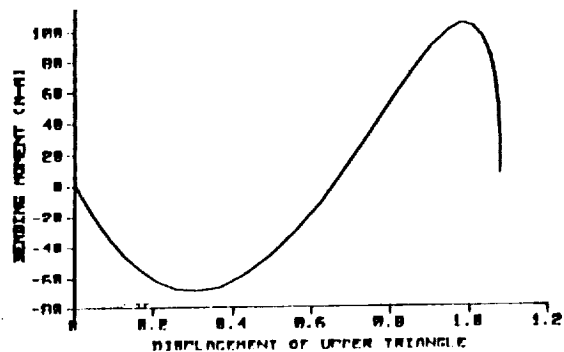


Figure 7 Bending Moment of the Longeron at Midpoint

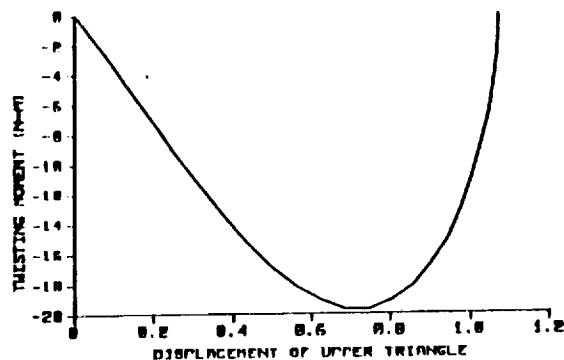


Figure 8 Twisting Moment of the Longeron

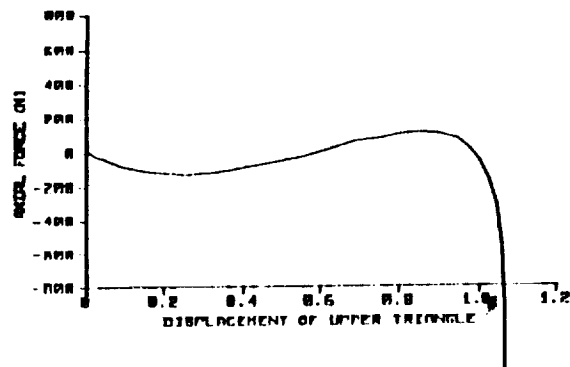


Figure 11 Axial Force of the Longeron

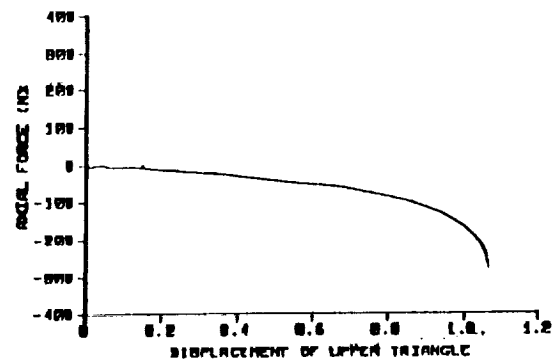


Figure 12 Axial Force of the Diagonal A

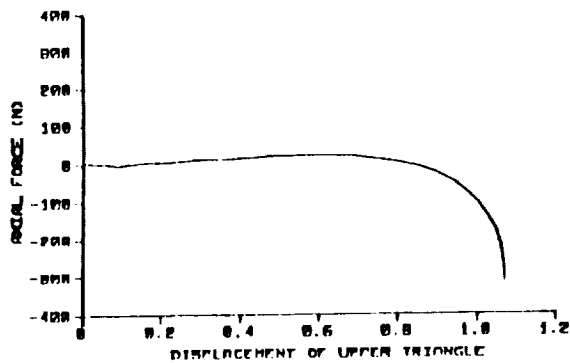


Figure 13 Axial Force of the Diagonal B

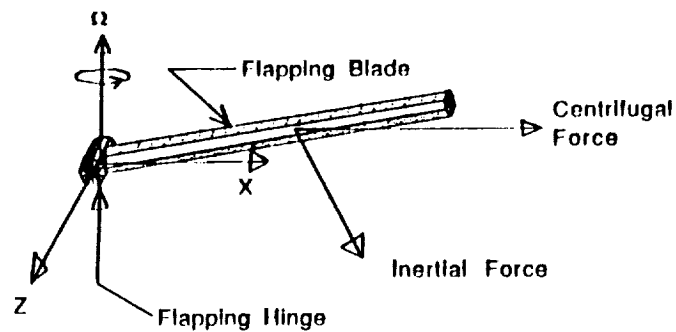


Figure 15 A Flapping Blade

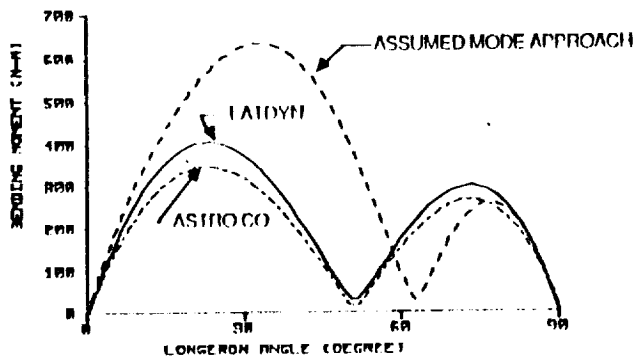


Figure 14 Bending Moment of the Longeron at Upper and

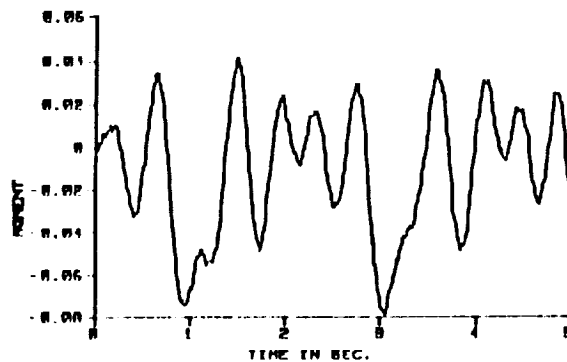


Figure 16 Flapping Bending Moment ($\Omega=3.0$ rad/sec)

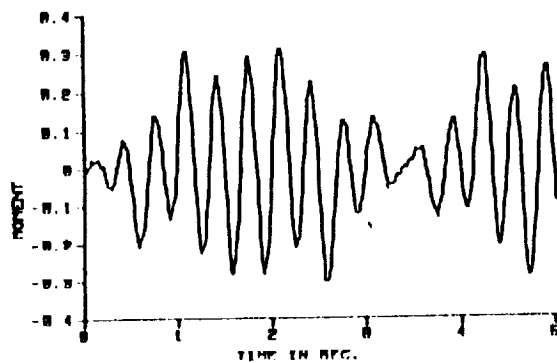


Figure 17 Flapping Bending Moment ($\Omega=6.0$ rad/sec)

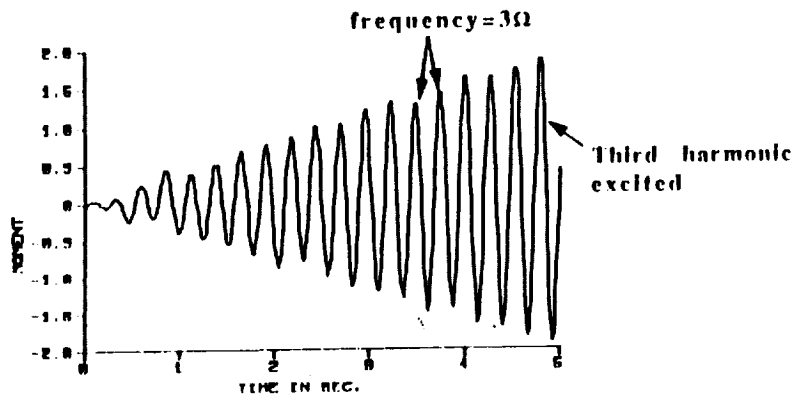


Figure 19 Resonance of Flapping Blade ($\Omega=8.0$ rad/sec)

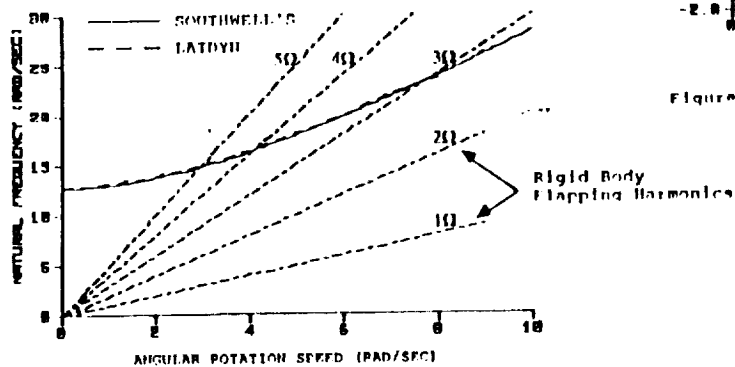


Figure 18 Coalescence of Flexible and Rigid Body Harmonics